

# Integrating Sbas-insar and Artificial Intelligence for Land Subsidence Monitoring in Ca Mau, Vietnam

HA Trung Khien<sup>1</sup>, TRAN Van Anh<sup>2,\*</sup>, PHAM Quy Nhan<sup>3</sup>, LUONG Ngoc Dung<sup>1</sup>, TRAN Dinh Trong<sup>1</sup>

<sup>1</sup> Hanoi University of Civil Engineering, Hanoi, Vietnam

<sup>2</sup> Hanoi University of Mining and Geology, Hanoi, Vietnam

<sup>3</sup> Hanoi University of Natural Resources and Environment, Hanoi, Vietnam

\* Corresponding author: [tranvananh@humg.edu.vn](mailto:tranvananh@humg.edu.vn)

**Abstract:** *In recent years, land subsidence has become a significant concern in the Ca Mau region, Vietnam, causing major environmental and socio-economic challenges. InSAR technology has been effectively applied in monitoring surface deformation over large areas. However, traditional InSAR processing methods still face limitations due to noise, phase unwrapping errors, and atmospheric disturbances, which affect the reliability of subsidence results. This study employs an integrated approach combining SBAS-InSAR with Artificial Intelligence (AI) to enhance the accuracy and efficiency of land subsidence monitoring. AI algorithms are applied to improve phase unwrapping, reduce noise, and correct atmospheric effects, thereby improving the quality of deformation signals obtained from InSAR data. The method is tested using Sentinel-1 imagery acquired over the Ca Mau city area during the period from January 2022 to December 2023. The results indicate that integrating AI significantly enhances the accuracy of land subsidence detection, achieving strong agreement with leveling subsidence data ( $R^2 = 0.80$ ; RMSE = 3 mm).*

**Keywords:** *Land subsidence; Artificial intelligence; InSAR; SBAS-InSAR; Phase filtering*

## 1. Introduction

In the field of radar remote sensing, Interferometric Synthetic Aperture Radar (InSAR) is a powerful technique for measuring surface deformation with high precision, thereby supporting the generation of Digital Elevation Models (DEMs) and monitoring topographic changes. However, one of the major challenges in processing SAR imagery is the presence of speckle noise and phase noise, which significantly degrade image quality and directly impact the accuracy of derived products such as DEMs and displacement maps. This noise arises from the random interference of coherent backscattered signals within each resolution cell, making accurate phase extraction particularly difficult, especially in areas with low coherence or dense interferometric fringes (Saied et al., 2020).

To mitigate noise in SAR interferograms, a variety of filtering techniques have been developed. Classical statistical filters such as Lee, Frost, and Kuan, based on the multiplicative noise model and local statistical estimation, are capable of smoothing homogeneous regions while preserving edges and dominant structures (Lee, 1980; Frost et al., 1982; Kuan et al., 1985). Subsequently, advanced adaptive approaches were introduced, including shape-adaptive filtering (Lopes et al., 1993), which adjusts the filtering window according to image morphology, and the Goldstein filter (Goldstein & Werner, 1998), which employs Fourier transform with a tunable  $\alpha$  parameter to enhance the signal-to-noise ratio. The non-local means method (Buades et al., 2005), exploiting similarity among distant patches, has demonstrated superior performance. Furthermore, transform-domain methods such as wavelet (Argenti & Alparone, 2002) and curvelet (Devapal et al., 2019) have been applied for multiscale denoising, enabling the preservation of details, edges, and fine structures in SAR imagery. More recently, improvements such as the AP-Goldstein filter (Chi et al., 2021) have been proposed, in which the filtering parameter is adaptively tuned according to local homogeneity and pseudo-coherence.

In recent years, numerous studies worldwide have employed deep learning and machine learning approaches to denoise SAR imagery and enhance phase filtering outcomes. Among pioneering deep learning models, Wang et al. (2017) proposed a CNN-based despeckling method for SAR imagery, incorporating batch normalization, ReLU activation, and residual component layers, which demonstrated superior denoising performance. DnCNN has demonstrated superior performance in removing speckle noise in amplitude images, thereby improving the quality of DEMs generated from SLC images (Saied et al., 2020). An improved non-local denoising algorithm for multi-baseline InSAR, combined with a non-

local probability density function and machine learning, is designed to achieve effective noise suppression while preserving detail and fringe continuity, particularly for interferograms with large baselines (Li & Yang, 2023). However, for InSAR phase denoising, the requirements for preserving fine details, edge structures, and phase continuity make the problem considerably more complex, necessitating more sophisticated and flexible models. An advanced approach in this domain is the MOMFNet model proposed by Zhang et al. (2024). MOMFNet is a fully convolutional deep learning architecture that integrates multi-scale feature extraction (MF-SENet) with channel attention mechanisms to enhance critical information within phase images. Notably, the model employs a multi-objective loss function to simultaneously preserve phase structure, edge characteristics, and statistical properties of the image. The training data were constructed using simulated deformation phases with Gaussian characteristics, fractal-based atmospheric noise, and complex Gaussian noise. Experimental results indicate that MOMFNet outperforms traditional methods such as DnCNN, BM3D, and the Goldstein filter, both in terms of denoising capability and detail preservation on simulated as well as real Sentinel-1 data. In parallel, other deep learning models have also been proposed to address the limitations in InSAR noise processing. PFCT and CNN architectures have been combined with Transformers to exploit both local and non-local features in phase images, improving noise suppression without destroying fringe structures (Wang et al., 2024). Another model,  $\Phi$ -Net, based on a U-Net architecture, enables effective phase denoising and high-accuracy coherence estimation, although high-frequency fringes may still emerge in heavily noisy regions (Akiki et al., 2024). Zhao et al. (2024) proposed an InSAR phase denoising network based on a multi-attention mechanism combined with a multi-objective loss function, which not only reduces noise but also preserves edge details, achieving superior performance compared to traditional methods on both simulated and real datasets. NBDNet adopts a self-supervised Neighbor2Neighbor learning framework, allowing model training on real interferograms without the need for clean ground-truth labels, while simultaneously estimating phase and coherence in both single-look and multi-look cases (Li et al., 2025). Another study applied a Semi-Supervised Self-Boosting Learning approach for InSAR phase denoising, enabling the model to leverage both simulated and real noise (Zhang et al., 2025).

In Vietnam, most current research efforts have predominantly focused on enhancing optical image quality, such as cloud removal, spatial resolution enhancement, or land cover classification (Dang et al., 2023; Do et al., 2022). Existing studies related to InSAR processing are largely limited to the application of traditional filtering techniques such as the Goldstein filter, Lee filter, Frost filter, or Gamma-Map for speckle and phase noise reduction (Pham et al., 2019). However, these studies have not systematically evaluated the effectiveness of different filtering methods, nor their impact on the accuracy of InSAR-derived products such as ground displacement maps or DEMs.

This study proposes a method for detecting land subsidence using the SBAS-InSAR technique, combined with phase noise filtering approaches to enhance the accuracy of interferometric images. Specifically, three filtering methods are compared and evaluated: the traditional Lee filter, the Goldstein filter, and the deep learning-based Restormer model — a modern Transformer architecture designed for high-resolution image restoration tasks. The integration of these filtering techniques into the SBAS-InSAR processing chain effectively suppresses phase noise while preserving edge features and interferometric fringes essential for surface deformation analysis.

## 2. Methodology

### 2.1. The SBAS-InSAR method

The Small Baseline Subset Interferometric Synthetic Aperture Radar (SBAS-InSAR) technique is an advanced method developed for detecting and quantifying ground surface deformation using time-series analysis of Synthetic Aperture Radar (SAR) data. Originally proposed by Berardino et al. (2002), SBAS-InSAR leverages interferometric pairs with small spatial and temporal baselines to minimize decorrelation effects and reduce phase errors caused by atmospheric delays and orbital inaccuracies.

Consider a set of  $N+1$  SAR images acquired over the same area at discrete times  $t_0, t_1, \dots, t_N$ . By applying specific thresholds to the spatial and temporal baselines, a total of  $M$  interferometric pairs can be generated, satisfying the condition:

$$\frac{N+1}{2} \leq M \leq \frac{N \cdot (N+1)}{2} \quad (1)$$

Assuming  $t_0$  as the reference acquisition time, the interferometric phase for any image pair captured at times  $t_A$  and  $t_B$  at pixel position  $(r, x)$  can be expressed as:

$$\begin{aligned} \delta\phi(r,x) &= \phi(t_A, r, x) - \phi(t_B, r, x) \\ &\approx \delta\phi_{\text{disp},i} + \delta\phi_{\text{topo},i} + \delta\phi_{\text{atm},i} + \delta\phi_{\text{noise},i} \end{aligned} \quad (2)$$

Here,  $\delta\phi_{\text{disp}}$  denotes the deformation-induced phase,  $\delta\phi_{\text{topo}}$  represents the residual topographic contribution,  $\delta\phi_{\text{atm}}$  is the atmospheric phase delay, and  $\delta\phi_{\text{noise}}$  accounts for random noise. After compensating for topographic, atmospheric, and noise components, the deformation phase can be approximated as:

$$\delta\phi_i(r,x) \approx \delta\phi_{\text{disp},i} = \frac{4\pi}{\lambda} [d(t_A, r, x) - d(t_B, r, x)] \quad (3)$$

Where  $\lambda$  is the radar wavelength, and  $d(t_A, r, x)$  and  $d(t_B, r, x)$  denote the cumulative Line-of-Sight (LOS) displacements at times  $t_A$  and  $t_B$ , respectively, relative to the reference.

These differential phases form a system of linear equations of the form:

$$A\phi = \delta\phi \quad (4)$$

Where  $A$  is the temporal design matrix representing the relationship between the interferometric pairs,  $\phi$  is the unknown phase vector at each acquisition time, and  $\delta\phi$  is the observed phase vector. Provided that  $A$  has full rank, the system can be resolved using the least-squares solution:

$$\phi = (A^T A)^{-1} A^T \delta\phi \quad (5)$$

## 2.2. The phase denoising techniques

### 2.2.1. The Lee filter

The Lee filter is an adaptive statistical method designed to reduce speckle noise in SAR and other coherent imaging systems while preserving structural details (Lee, 1980). It operates based on local statistics computed within a moving window centered on each pixel.

Within each window, the local mean ( $\bar{I}$ ) and local variance ( $v$ ) are used to estimate the statistical behavior of the target pixel. The filtered pixel value is computed as:

$$I_f = \bar{I} + W \times (I - \bar{I}) \quad (6)$$

Where  $I$  is the original pixel,  $I_f$  is the filtered value, and  $W$  is a weight factor. The value of  $W$  depends on the noise characteristics and the desired processing goal.

For contrast enhancement,  $W = k = \sigma_c / \sigma$ , where the ratio of local standard deviations determines the level of smoothing or sharpening. where  $\sigma_c$  and  $\sigma$  denote the adjusted and original standard deviations, respectively. If  $k > 1$ , the image is sharpened (akin to high-pass filtering); if  $0 \leq k < 10$ , the image is smoothed (similar to low-pass filtering). When  $k = 0$ , the output equals the local mean, resulting in significant blurring.

For additive noise,  $W$  is computed as:

$$W = \frac{Q}{Q + \sigma_w^2} \quad (7)$$

Where  $Q$  is the signal variance and  $\sigma_w^2$  is the noise variance. Similar formulations apply to multiplicative or mixed noise models.

The filter processes each pixel independently without requiring complex transforms, making it suitable for real-time and parallel processing. The window size affects the trade-off between smoothing and detail preservation; typical sizes range from  $3 \times 3$  to  $7 \times 7$ , depending on the application.

In InSAR applications, the Lee filter can be applied to magnitude images, phase images, or complex-valued images. Notably, extended versions such as the complex Lee filter enable direct filtering of complex interferograms, thereby improving the quality of the interferometric phase while preserving its accuracy. This enhancement contributes significantly to the reliable extraction of surface deformation information.

### 2.2.2. The Goldstein filter

The Goldstein filter is an adaptive filtering technique specifically designed to suppress phase noise in synthetic aperture radar (SAR) interferograms (Goldstein & Werner, 1998). These interferograms typically contain a power spectrum composed of two main components: a narrowband signal corresponding to the interferometric fringes and deformation information, and a broadband noise component attributed to thermal noise, temporal decorrelation, and geometric variations in the baseline.

The filtering mechanism operates in the frequency domain. Initially, the interferogram  $I(x,y)$  is divided into overlapping rectangular blocks. For each block, the power spectrum  $Z(u,v)$  is computed as the squared magnitude of the two-dimensional Fast Fourier Transform (FFT), often followed by spectral smoothing to enhance stability. The adaptive filter response  $H(u,v)$  is then defined as:

$$H(u,v)=|Z(u,v)|^a \tag{8}$$

Where  $a$  is a tunable parameter controlling the filtering strength. Typically, a range from 0.2 to 1. When  $a = 0$ , no filtering is applied; when  $a = 1$ , the filter applies maximum attenuation to the noise. In practice, interferograms with lower coherence benefit from larger block sizes and higher values of  $a$  to enhance filtering performance. The blocks are overlapped by 75% in both azimuth and range directions, and a triangular weighting function is applied to reduce boundary artifacts between blocks.

A key feature of the Goldstein filter is its spatial adaptivity. It applies strong filtering in regions with low phase variation (smooth fringes) and weaker filtering in areas of high phase variance, such as those affected by deformation or noise. This behavior results from the filter's variable bandwidth, derived directly from the local power spectrum. It enables the preservation of critical high-frequency information in complex regions while effectively smoothing homogeneous areas.

### 2.2.3. Restormer model

The Restormer model is developed by modifying and enhancing the core components of the conventional Transformer architecture to better address the challenges of high-resolution image restoration (Zamir et al., 2022). Its primary innovation lies in the restructuring of the self-attention mechanism and the feed-forward network, aiming to reduce computational complexity while still effectively capturing both local details and long-range dependencies among pixels.

In Restormer, each Transformer block is designed to sequentially apply two key modules—Multi-Dconv Head Transposed Attention (MDTA) and Gated-Dconv Feed-Forward Network (GDFN)—with the integration of residual connections and layer normalization to enhance stability and representational depth. The mathematical formulation of a single block can be expressed as a two-stage residual operation.

Let  $X \in \mathbb{R}^{H \times W \times C}$  denote the input feature tensor to a Transformer block. The first operation is MDTA, which refines the input features using global contextual information across channels. Prior to applying MDTA, the input is normalized via Layer Normalization (LN), and the output of MDTA is added back to the input through a residual connection:

$$Z_1 = \text{MDTA}(\text{LN}(X)) + X \tag{9}$$

The second operation involves the GDFN module, which applies a gated feed-forward transformation to the intermediate output  $Z_1$ . Again, layer normalization is applied before the transformation, followed by another residual connection:

$$Z_2 = \text{GDFN}(\text{LN}(Z_1)) + Z_1 \tag{10}$$

This two-step formulation allows each Transformer block to progressively refine features by modeling both non-local dependencies and spatially-aware feed-forward mappings. The residual design ensures better gradient flow during training and helps the network to preserve important structural information from earlier layers.

By stacking such blocks within an encoder-decoder framework and combining them with multi-scale representations, Restormer effectively learns rich contextual features suitable for complex image restoration tasks.

### 3. Materials and experiments

#### 3.1. Data

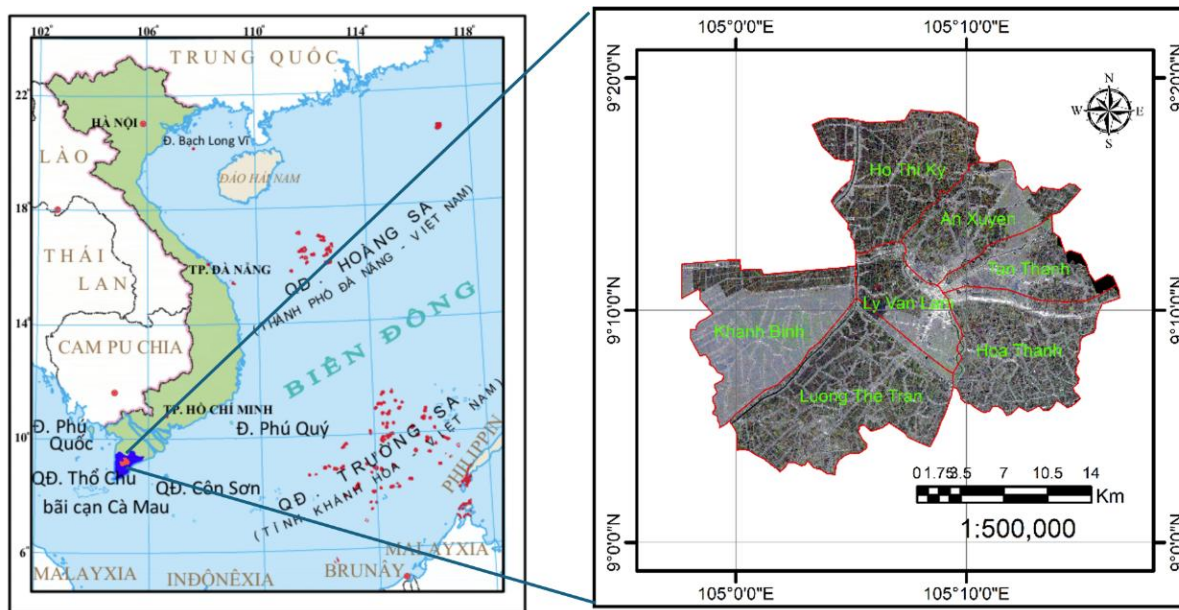


**Fig. 1.** Study area

In this study, a total of 24 Sentinel-1A radar scenes acquired from January 2022 to December 2023 were used to cover the entire study area. Sentinel-1A is a satellite under the Copernicus Earth Observation Program operated by the European Space Agency (ESA), equipped with a C-band Synthetic Aperture Radar (SAR) operating in Interferometric Wide Swath (IW) mode with VV polarization and a 12-day repeat cycle. The Sentinel-1A datasets were obtained from the Alaska Satellite Facility's database (<https://search.asf.alaska.edu/>). In addition, Shuttle Radar Topography Mission (SRTM) digital elevation model (DEM) data with a spatial resolution of 30 meters, provided by NASA, was used for topographic correction in the InSAR processing workflow.

The study area encompasses the entire administrative region of 7 wards and communes in the central part of Ca Mau Province, including the wards of Ly Van Lam, Hoa Thanh, Tan Thanh, and An Xuyen; along with the communes of Ho Thi Ky, Khanh Binh, Luong The Tran. The topography of the area is predominantly flat, with an average elevation ranging from 0.4 to 0.6 meters above sea level. Some low-lying regions have elevations around 0.2 meters, whereas higher areas may reach between 0.8 and 1.1 meters. The general terrain shows a gentle slope trending from north to south and northeast to southwest.

#### 3.2. Experimental workflow

This study was conducted using 24 Sentinel-1A SAR scenes covering the study area from January 2022 to December 2023, aiming to analyze ground surface deformation through the SBAS-InSAR technique. Interferograms were generated from image pairs with small spatial and temporal baselines and subsequently denoised using three different phase filtering methods to enhance phase quality: Lee filter, Goldstein filter, and a deep learning-based Restormer model.

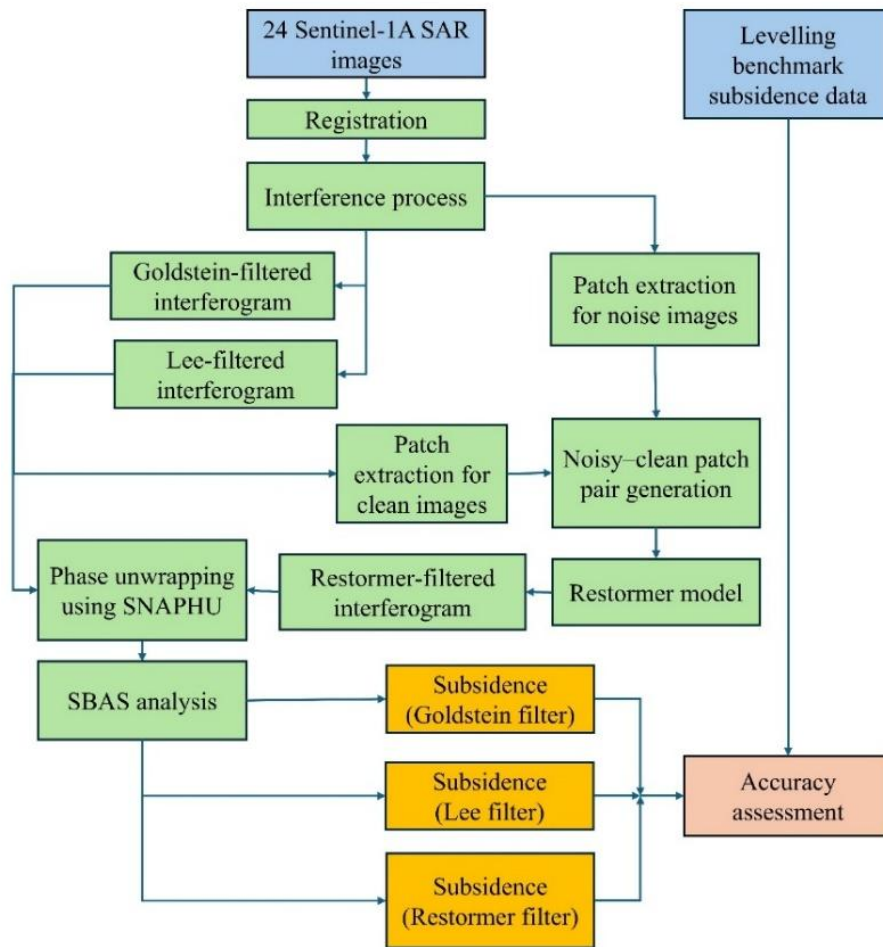


**Fig. 2.** Workflow of SBAS-InSAR analysis with Lee, Goldstein, and Restormer filtering.

The processing workflow includes the following main steps (Fig. 2):

Step 1: A total of 24 Sentinel-1A SAR images acquired between January 2022 and December 2023 were selected for analysis.

Step 2: All images were co-registered with sub-pixel accuracy using geometric correction techniques. Radiometric calibration and initial noise filtering were also applied to improve image quality and ensure high coherence between image pairs.

Step 3: Interferometric pairs were generated based on small spatial and temporal baselines to minimize decorrelation. Differential interferograms were then computed and corrected for orbital and atmospheric phase errors.

Step 4: A phase denoising step was applied to reduce noise and enhance phase continuity before unwrapping. Three filtering methods were employed for comparative analysis: (i) the Lee filter, a statistical adaptive filter that suppresses speckle noise while preserving important phase features; (ii) the Goldstein filter, which operates in the frequency domain and enhances interferometric fringe visibility; and (iii) a Restormer-based deep learning model, trained using 9,716 pairs of noisy and clean patches. The clean patches were generated from interferograms filtered separately by the Lee and Goldstein methods, forming a diverse and representative training dataset for learning phase denoising patterns.

Step 5: The denoised interferograms were unwrapped using the SNAPHU (Statistical-Cost Network-Flow Algorithm for Phase Unwrapping) algorithm (Chen & Zebker, 2000) to convert wrapped phase values into continuous phase measurements.

Step 6: A Digital Elevation Model (DEM) was used to remove residual topographic phase components. Finally, the SBAS algorithm was applied to the time series of unwrapped interferograms to estimate ground deformation over the study area. The ground deformation results were evaluated for accuracy by comparing them with leveling subsidence data.

#### 4. Results and Discussion

A total of 24 SAR scenes, following preprocessing procedures including image co-registration and geometric correction, were utilized to generate 66 interferometric pairs using the PyGMTSAR library (Pechnikov, 2023) on the Google Colab platform. The baseline network of these interferometric pairs is depicted in Figure 3.

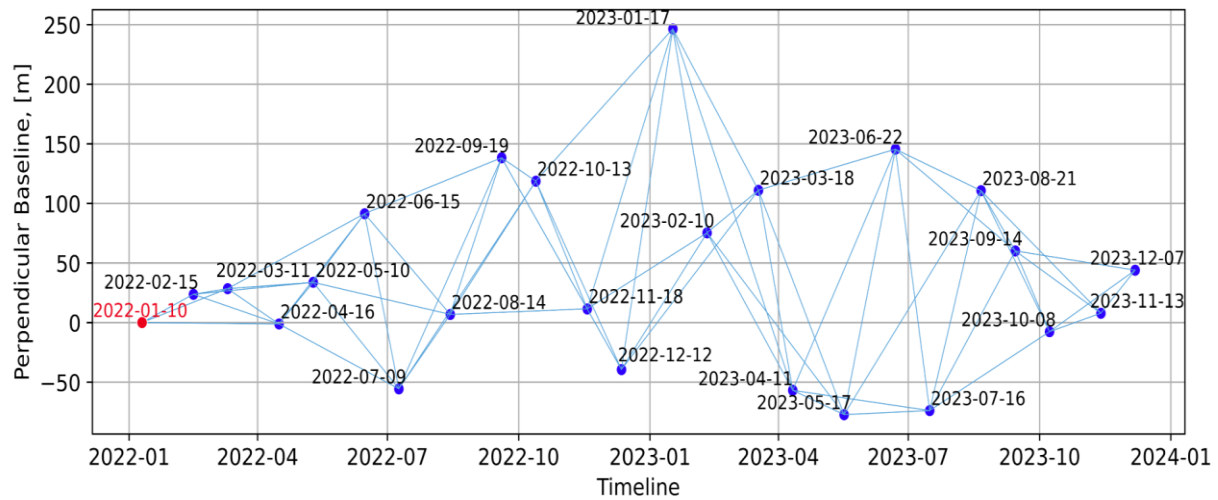


**Fig. 3.** Distribution diagram of the baseline set of Sentinel-1A images

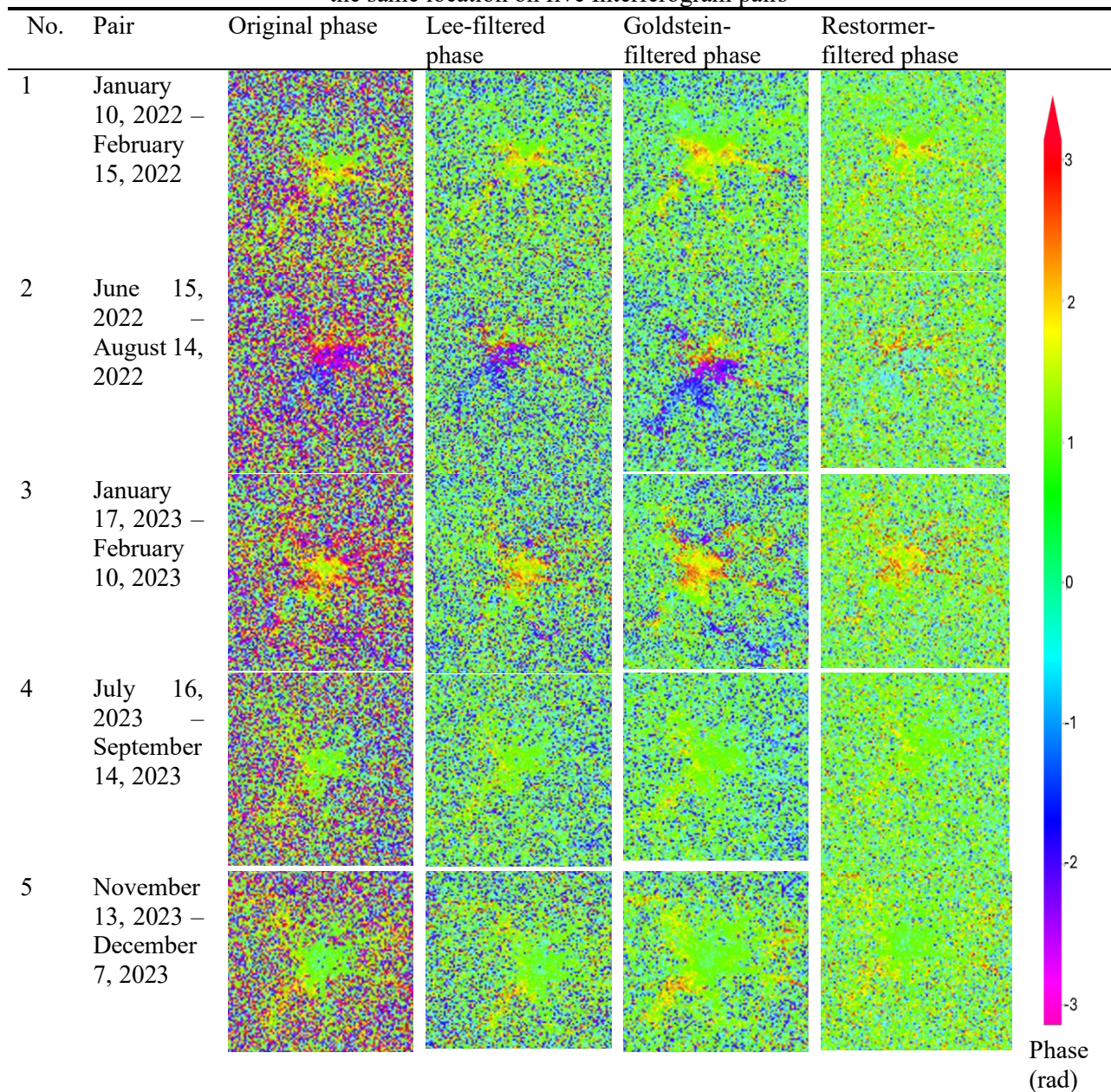
After generating interferograms from SAR image pairs using the PyGMTSAR library (Pechnikov, 2023) on the Google Colab platform, phase denoising was carried out using three different methods: the Lee filter, the Goldstein filter, and the deep learning-based Restormer model. Table 1 presents a visual comparison of the filtering results at the same location across five representative interferogram pairs. Qualitative assessment indicates that the Restormer model provides stronger noise suppression, as evidenced by smoother and clearer interferometric phase patterns compared to the traditional Lee and Goldstein filters. However, to verify the reliability and phase preservation capability of each filtering method, further processing steps such as phase unwrapping and subsidence estimation are required for a more comprehensive evaluation.

Following denoising using three distinct methods—the Lee filter, the Goldstein filter, and the deep learning-based Restormer model—all 66 interferometric pairs undergo phase unwrapping with the SNAPHU software to retrieve continuous phase information. The resulting unwrapped phase data are then integrated into the SBAS-InSAR processing chain to analyze ground deformation and estimate temporal subsidence patterns with improved accuracy.

Figure 4 presents the estimated ground subsidence at the final epoch of the SBAS-InSAR processing chain, corresponding to three different phase filtering approaches: the Lee filter, the Goldstein filter, and the deep learning-based Restormer model. The results demonstrate a high level of consistency in identifying major subsidence areas across all three methods. This indicates that the key phase information relevant to deformation analysis is well preserved, and highlights the potential of the Restormer model as a viable alternative to traditional filters while maintaining reliable subsidence estimation performance.

To verify the reliability of surface subsidence results derived from the SBAS method using three different phase filtering techniques, the study conducted a comparison with ground-truth measurements at 11 benchmark locations (Fig. 3b). At these sites, subsidence was determined through high-precision leveling surveys carried out by the Department of Survey, Mapping and Geographic Information of Vietnam (Tran et al., 2024). This comparison, illustrated in Table 2, enables an assessment of the consistency between InSAR-derived results and conventional geodetic measurements, thereby validating the effectiveness of each filtering method in preserving phase information for deformation analysis.

**Tab. 1.** Comparison of phase filtering results of three methods at the same location on five Interferogram pairs



**Tab. 2.** Comparison of subsidence estimated by SBAS-InSAR using three filtering methods (Lee, Goldstein, and Restormer model) with leveling measurements

No.	Point name	Vertical displacement from SBAS-InSAR (mm)			Leveling-measured subsidence (mm)	Difference compared to leveling-measured subsidence (mm)		
		Goldstein	Lee	Restormer		Goldstein	Lee	Restormer
1	II(CM-TVT)3	-7	-16	-12	-10	3	-6	-2
2	II(CM-TVT)2	-8	-15	-13	-11	3	-4	-2
3	II(SC-PL)24	-30	-35	-20	-25	-5	-10	5
4	II(SC-PL)25A	-25	-15	-20	-23	-2	8	3
5	II(SC-PL)27	-28	-35	-28	-24	-4	-11	-4
6	II(SC-PL)28	-16	-20	-18	-15	-1	-5	-3
7	III(HS-CM)5	-9	-15	-10	-8	-1	-7	-2
8	III(HS-CM)6	-15	-10	-10	-8	-7	-2	-2
9	III(HS-CM)8	-17	-17	-8	-10	-7	-7	2

No.	Point name	Vertical displacement from SBAS-InSAR (mm)			Leveling-measured subsidence (mm)	Difference compared to leveling-measured subsidence (mm)		
		Goldstein	Lee	Restormer		Goldstein	Lee	Restormer
10	III(HS-CM)9	-7	-20	-17	-14	7	-6	-3
11	III(TV-PU)5	-13	-22	-8	-10	-3	-12	2

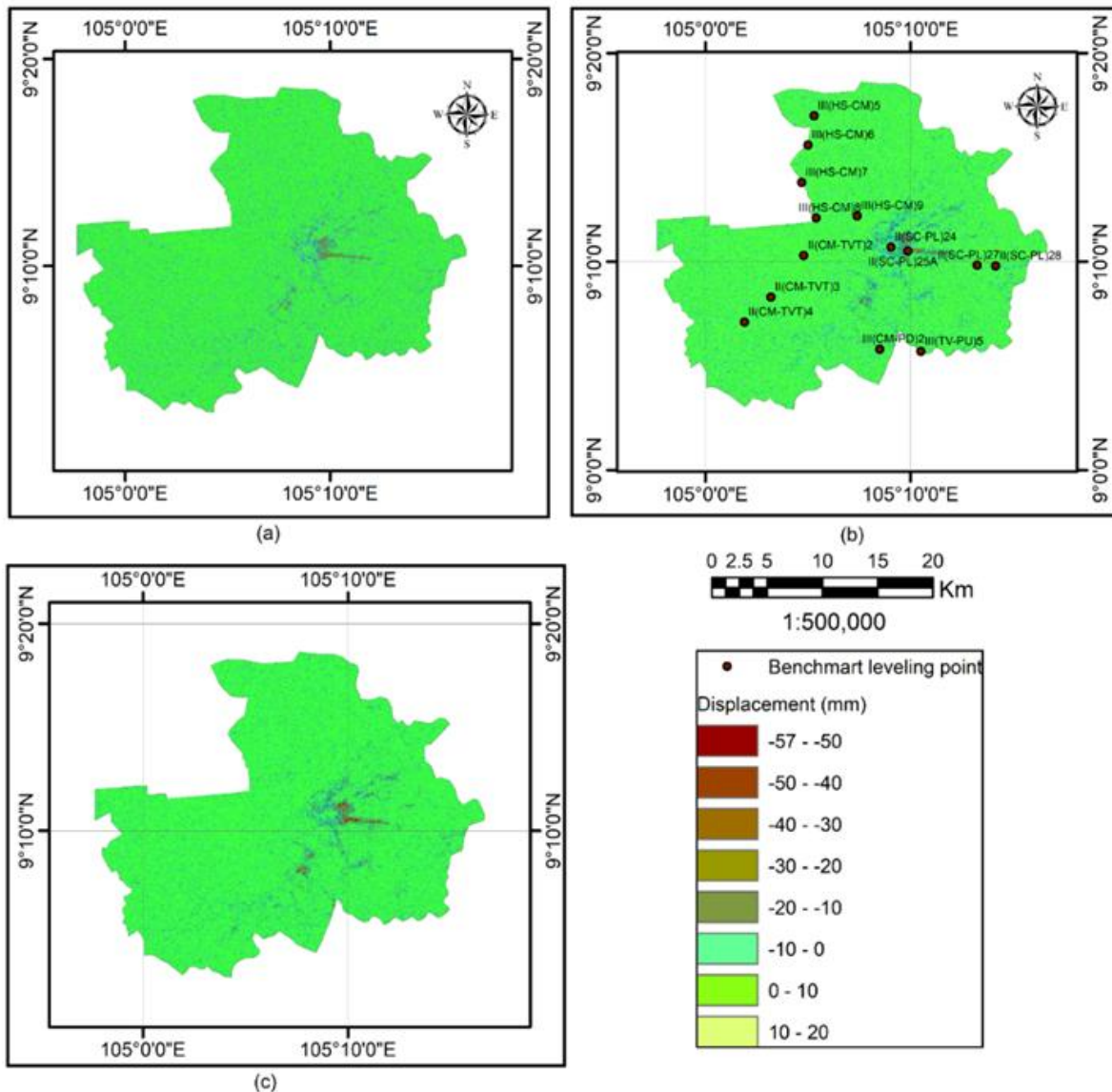


**Fig. 4.** Comparison of subsidence maps using different filtering methods: (a) Lee filter, (b) Restormer model, and (c) Goldstein filter

The study employed linear regression to evaluate the correlation between surface subsidence results obtained from the SBAS-InSAR method using three different phase filtering techniques and field measurements conducted by leveling. The results indicate that the deep learning-based Restormer filtering method achieved the highest accuracy among the three techniques. The superior performance of the deep learning-based Restormer filtering method can be attributed to its ability to learn complex spatial and contextual features from interferometric data, rather than relying on fixed statistical assumptions as in traditional filters. While classical approaches such as Lee or Goldstein filters primarily operate under local statistical models and may oversmooth fringes or fail to suppress noise effectively in areas with low coherence, Restormer leverages a transformer-based architecture to capture long-range dependencies and preserve both local details and global phase continuity. This enables more accurate separation of signal and noise, resulting in cleaner interferograms that better maintain fringe structures. Consequently, the subsidence estimates derived from Restormer-filtered interferograms exhibited the strongest agreement

with leveling data, as reflected in the highest correlation coefficient ( $R^2 = 0.80$ ) and the lowest RMSE of 3 mm (Fig. 5).

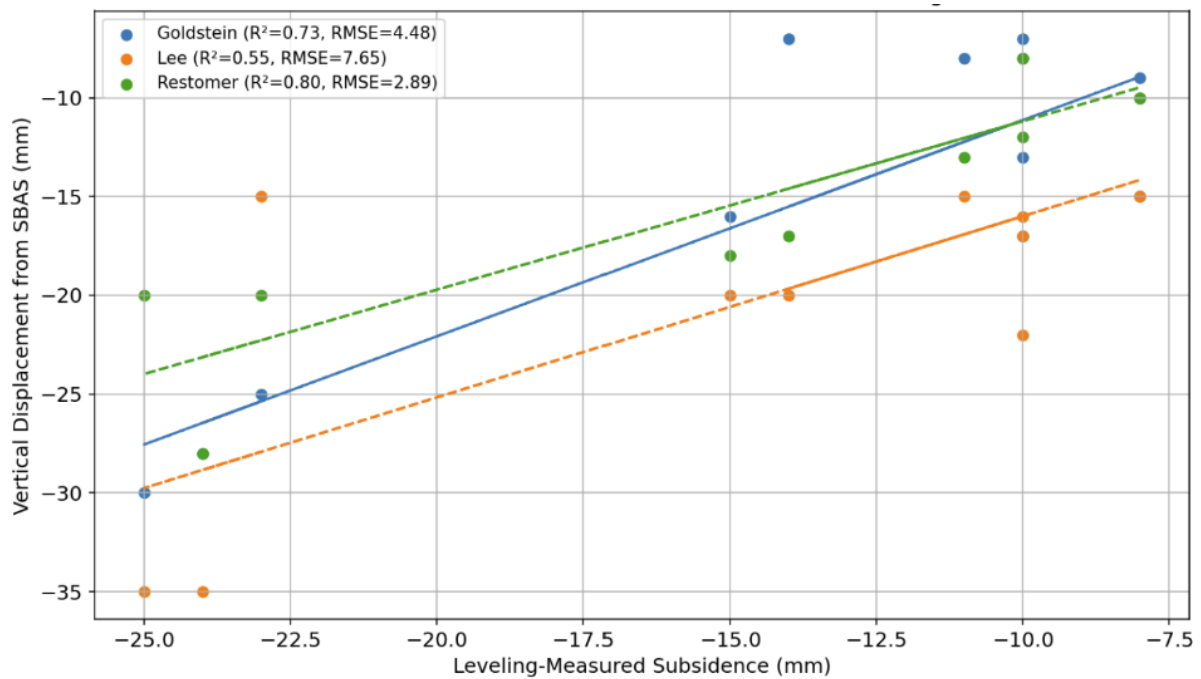


**Fig. 5.** Assessment of the correlation between ground subsidence data derived from SBAS-InSAR using three filtering methods (Lee, Goldstein, and Restormer) and leveling measurements

### 5. Conclusion

This study demonstrates the potential of integrating advanced phase filtering techniques, particularly deep learning-based models, into the SBAS-InSAR processing workflow to improve the accuracy of ground deformation monitoring. By utilizing 24 Sentinel-1A SAR scenes from 01/2022 to 12/2023 and applying three different filtering methods—Lee, Goldstein, and Restormer—on interferograms generated using PyGMTSAR, the study found that the Restormer model offers superior denoising performance. Qualitative visual comparisons and quantitative correlation analyses with leveling data confirm that Restormer not only enhances phase quality but also preserves deformation signals more effectively than traditional filters. The strong agreement with ground truth data ( $R^2 = 0.80$ , RMSE = 3 mm) highlights the advantages of incorporating deep learning into InSAR workflows. These findings support the adoption of AI-assisted filtering techniques for more reliable and precise land subsidence assessment in vulnerable regions such as Ca Mau.

### References

Akiki, R.; Anger, J.; de Franchis, C.; Facciolo, G.; Grandin, R.; Morel, J.-M. (2024). A Brief Evaluation of InSAR Phase Denoising and Coherence Estimation with Phi-Net, *Image Processing On Line* 14, p. 205.

Argenti, F.; Alparone, L. (2002). Speckle removal from SAR images in the undecimated wavelet domain, *IEEE TGRS* 40(11), p. 2363.

Berardino, P.; Fornaro, G.; Lanari, R.; Sansosti, E. (2002). A new algorithm for surface deformation monitoring based on small baseline differential SAR interferograms, *IEEE Trans. Geosci. Rem. Sens.* 40, p. 2375.

Buades, A.; Coll, B.; Morel, J.-M. (2005). A non-local algorithm for image denoising, *CVPR* 2, p. 60.

Chen, C.W.; Zebker, H.A. (2000). Network approaches to two-dimensional phase unwrapping: intractability and two new algorithms, *Journal of the Optical Society of America A* 17(3), p. 401.

Chi, B.; Zhuang, H.; Fan, H.; Yu, Y.; Peng, L. (2021). An adaptive patch-based Goldstein filter for interferometric phase denoising, *IJRS* 42(17), p. 6746.

Dang, T.T.; Hoang, T.T.; Ta, M.N. (2023). Application of satellite images and artificial intelligence to monitor land cover changes in Hanoi area during 2013–2023 period, *VNU Journal of Science: Earth and Environmental Sciences* 39(4).

- Devapal, D.; Hashna, N.; Aparna, V.P.; Bhavyasree, C.; Mathai, J.; Soman, K.S. (2019). Object detection from SAR images based on curvelet despeckling, *Materials Today: Proceedings* 11(3), p.1102.
- Do, T.N.; Pham, V.D.; Bui, Q.T.; Pham, V.M. (2022). Study model for information reconstruction on cloud contaminated area for single multispectral remote sensing Sentinel-2 imagery using generative adversarial network, *VNU Journal of Science: Earth and Environmental Sciences* 38(3), p. 32.
- Frost, V.S.; Stiles, J.A.; Shanmugan, K.S.; Holtzman, J.C. (1982). A model for radar images and its application to adaptive digital filtering of multiplicative noise, *IEEE TPAMI* 4(2), p. 157.
- Goldstein, R.M.; Werner, C.L. (1998). Radar interferogram filtering for geophysical applications, *Geophysical Research Letters* 25(21), p. 4035.
- Kuan, D.T.; Sawchuk, A.A.; Strand, T.C.; Chavel, P. (1985). Adaptive noise smoothing filter for images with signal-dependent noise, *IEEE TPAMI* 7(2), p. 165.
- Lee, J.S. (1980). Digital image enhancement and noise filtering by use of local statistics, *IEEE Transactions on Pattern Analysis and Machine Intelligence PAMI-2* (2), p. 165.
- Li, H.; Wang, J.; Ai, C.; Wu, Y.; Ren, X. (2025). NBDNet: A Self-Supervised CNN-Based Method for InSAR Phase and Coherence Estimation, *Remote Sensing* 17(7), p. 1181.
- Li, X.; Yang, T. (2023). A novel non-local denoising filter based on multibaseline InSAR, *IEEE Journal on Miniaturization for Air and Space Systems* 4(4), p. 376.
- Lopes, A.; Nezry, E.; Touzi, R.; Laur, H. (1993). Structure detection and statistical adaptive speckle filtering in SAR images, *IJRS* 14(9), p. 1735.
- Mukherjee, S.; Zimmer, A.; Kottayil, N.K.; Sun, X.; Ghuman, P.; Cheng, I. (2018). CNN-based InSAR denoising and coherence metric, *IEEE Sensors*. New Delhi, India, p. 1.
- Pechnikov, A. (2023). *PyGMTSAR: Sentinel-1 Python InSAR: An Introduction*. Kindle Edition.
- Pham, M.V.; Pham, T.M.; Vu, V.D.Q.; Bui, Q.-T.; Tran, A.V.; Pham, H.M.; Nguyen, T.N. (2019). Integrating Sentinel-1A SAR data and GIS to estimate aboveground biomass and carbon accumulation for tropical forest types in Thuan Chau district, Vietnam, *Remote Sensing Applications: Society and Environment* 14, p. 148.
- Saied, H.; Ismail, M.; Saied, A.; Bassyoni, M. (2020). Improving DEM generation from SAR images using CNN-based despeckling, *International Journal of Remote Sensing* 41(23), p. 9037.
- Tran, A.V.B.; Ha, K.T.; Khuc, D.T.; Tran, D.N.; Tran, H.H.; Le, N.T. (2024). Land Subsidence Susceptibility Mapping in Ca Mau Province, Vietnam, Using Boosting Models, *ISPRS Int. J. Geo-Inf.* 13, p. 161.
- Wang, J.; Liu, J.; Ling, X.; Duan, Z. (2024). Deep Learning-Based Joint Local and Non-local InSAR Image Phase Filtering Method, *Geomatics and Information Science of Wuhan University*.
- Wang, P.; Zhang, H.; Patel, V.M. (2017). SAR image despeckling using a convolutional neural network, *IEEE SPL* 24(12), p. 1763.
- Zamir, S.W.; Arora, A.; Khan, S.; Hayat, M.; Khan, F.S.; Yang, M.H. (2022). Restormer: Efficient transformer for high-resolution image restoration, *IEEE/CVF Comput. Pattern Recognit.*, p. 5728.
- Zhang, Q.; Jiang, H.; Wang, T. (2025). A semi-supervised self-boosting learning method for InSAR phase denoising, *IEEE Transactions on Geoscience and Remote Sensing* 63, p. 1.
- Zhang, X.; Peng, C.; Li, Z.; Zhang, Y.; Liu, Y.; Wang, Y. (2024). MOMFNet: A Deep Learning Approach for InSAR Phase Filtering Based on Multi-Objective Multi-Kernel Feature Extraction, *Sensors*. 24(23), p. 7821.
- Zhao, T.; Fan, H.; Tian, Z.; Xin, J. (2024). A CNN based on multiple attention mechanisms for InSAR phase denoising, *IEEE Geoscience and Remote Sensing Letters* 21, p. 1.

